Research Square

Preprints are preliminary reports that have not undergone peer review.
They should not be considered conclusive, used to inform clinical practice,
or referenced by the media as validated information.

Dual-Time-Point Diagnostic 18F-FDG PET/MRI with 3-hour Delayed, Prone, Breast-Coil Acquisition for Characterization of BI-RADS 4 Nodules: A Single-Centre Diagnostic Accuracy Study

rui xu

xurui@qdu.edu.cn

Qingdao University https://orcid.org/0000-0002-4576-2872

Yong Fu Su

Qingdao University

Peng Yun Shi

Sichuan Taikang Hospital

Hao Shi

First Affiliated Hospital of Shandong First Medical University

Research Article

Keywords: breast nodule, PET/MRI, dual-time-point, delayed imaging, ADC, SUVmax

Posted Date: November 11th, 2026

DOI: https://doi.org/10.21203/rs.3.rs-11311013/v1

License: This work is licensed under a Creative Commons Attribution 4.0 International License.
Read Full License

Dual-Time-Point Diagnostic ^{18}F-FDG PET/MRI with 3-hour Delayed, Prone, Breast-Coil Acquisition for Characterization of BI-RADS 4 Nodules: A Single-Centre Diagnostic Accuracy Study

Su Fuyong[1,2], Shi Yunpeng[3], Shi Hao[4], Xu Rui[5]*

[1]Department of Radiological Medicine, School of Basic Medical Sciences, Qingdao University，Qingdao, Shandong Province, China

[2]Department of Nuclear Medicine, Sunshine Union Hospital, Weifang, Shandong Province, China

[3]Department of Nuclear Medicine, Sichuan Taikang Hospital，Chengdu, Sichuan Province, China

[4]Department of Nuclear Medicine, the First Affiliated Hospital of Shandong First Medical University，Taishan, Shandong Province, China

[5]Department of Interventional Medicine, the Affiliated Hospital of Qingdao University, Qingdao, Shandong Province, China

*Correspondence: Xu Rui (xurui@qdu.edu.cn)

1 Abstract

Objective: Conventional PET/MRI often misclassifies BI-RADS 4 breast nodules because of high parenchymal metabolic background, coil-related ADC distortion and

missed low-grade cancers. To evaluate the diagnostic performance of a combined multi-sequence dual-phase modular scanning (MSDP-MS) dataset integrating 3-h delayed ^{18}F-FDG PET with prone dedicated-breast-coil MRI, compared with early-phase supine-coil PET/MRI in BI-RADS 4 breast nodules.

Subjects and methods: 68 women with BI-RADS 4 breast nodules were enrolled and underwent PET/MRI examinations from July 2020 to February 2025. All examinations were performed on a GE SIGNA 3.0 T integrated PET/MRI system. Image post-processing was performed on an AW 4.6 workstation. After ^{18}F-FDG injection, patients rested in a dim quiet room. Whole-body supine PET/MRI was performed using a 16-channel torso coil. PET acquisition duration was 8 min and total whole-body scan duration was 40 min. At approximately 3 h post-injection, a delayed targeted acquisition was performed for suspected nodules and metabolically- active lesions. The patient was positioned prone, with breasts placed within an 8- channel dedicated breast coil. PET acquisition lasted 8 min and additional MRI sequences added approximately 12 min of table-time. Two breast radiologists independently interpreted lesion findings, with histopathology serving as the reference standard.

Results: Among the 68 lesions, 24 were malignant and 44 were benign. Compared with early-only conventional PET/MRI, the combined MSDP-MS dataset yielded accuracy 94.1 % vs 82.4 % ($P = 0.025$), sensitivity 91.7 % vs 75.0 % ($P = 0.041$), specificity 95.5 % vs 86.4 % ($P = 0.108$). Malignant lesions demonstrated lower ADCmin values irrespective of ^{18}F-FDG uptake trend. Exploratory optimal subgroup-specific ADCmin thresholds were 0.86×10^{-3} mm²/s (SUV-increase

subgroup) and 1.31×10^{-3} mm²/s (SUV-decrease subgroup). The additional delayed-phase imaging component added approximately 12 min of scanner table-time and improved overall diagnostic accuracy by 11.8 %, raising sensitivity to 91.7 %.

Conclusion: The combined MSDP-MS multiparametric dataset showed promising diagnostic performance for differentiating benign from malignant BI-RADS 4 breast nodules.

Key words: breast nodule; PET/MRI; dual-time-point; delayed imaging; ADC; SUVmax

2 Introduction

Breast nodules are common in women. Although most nodules are benign, accurate early lesion characterization is crucial for breast cancer treatment and prognosis [1]. Mammography, ultrasound, and MRI each have distinct advantages and limitations for evaluating breast lesions [2-4]. Hybrid PET/MRI combines the high metabolic sensitivity of positron-emission tomography (PET) with excellent soft-tissue contrast from magnetic resonance imaging (MRI), providing comprehensive diagnostic information [5,6]. However, standard single-time-point whole-body PET/MRI acquired approximately 60 min after ^{18}F-FDG injection frequently cannot capture dynamic metabolic behaviour, reliable apparent diffusion coefficient (ADC) measurements, or high-resolution anatomical details of breast lesions, which may contribute to diagnostic misclassification [5,6]. Systemic investigations addressing these limitations remain scarce. Prior groups have described prone dedicated-breast-coil PET/MRI protocols. The present work explores a 3-hour

delayed-time-point combined multiparametric workflow for BI-RADS 4 nodule characterization.

We retrospectively studied 68 women with BI-RADS 4 breast nodules who underwent PET/MRI examinations in our hospital between July 2020 and February 2025. The objective was to assess the diagnostic value of a modular dual-time-point dataset (multi-sequence dual-phase modular scanning, MSDP-MS), which added a delayed prone dedicated-breast-coil acquisition, compared with conventional early-phase supine whole-body PET/MRI.

3 Materials and Methods

3.1 Study Subjects

68 women with BI-RADS 4 breast nodules were enrolled.

Inclusion criteria:

1. Breast nodule classified as BI-RADS 4 on ultrasound or mammography.

2. Complete conventional early-phase plus delayed-phase MSDP-MS PET/MRI examinations available.

3. Histopathological reference standard obtainable for the target lesion.

Exclusion criteria: pregnancy, lactation, breast implants, claustrophobia, prior breast biopsy, neoadjuvant therapy, absence of histopathological outcome.

This study used existing clinical imaging and histopathological data and was approved by the Institutional Review Board of Sunshine Union Hospital (No 2025081316). The institutional review board waived the requirement for additional research-specific written informed consent. All patients had provided

routine clinical written consent for the PET/MRI examinations. All patient-identifying information was fully de-identified before analysis. The study was performed in accordance with the Declaration of Helsinki.

3.2 Imaging Protocol

All examinations were performed on a GE SIGNA 3.0 T integrated PET/MRI system. Image post-processing was performed on an AW 4.6 workstation. ^{18}F-FDG (radio chemical purity > 95 %) was produced using a GE MiniTrace cyclotron. Patients fasted for at least 6 h before injection and blood-glucose values were recorded. Intravenous ^{18}F-FDG was administered using weight-based dosing.

3.2.1 Conventional PET/MRI Imaging

After ^{18}F-FDG injection, patients rested in a dim quiet room. Whole-body supine PET/MRI was performed using a 16-channel torso coil (3.0 T UAA). PET acquisition duration was 8 min and total whole-body scan duration was 40 min. MRI sequences and parameters are summarised in Table 1. 3**.2.2 MSDP-MS**

The early-phase acquisition was identical to the conventional protocol described above. At approximately 3 h post-injection, a delayed targeted acquisition was performed for suspected nodules and metabolically-active lesions. The patient was positioned prone, with breasts placed within an 8-channel dedicated breast coil (3.0 T HD Flat GEM Table Breast Array). PET acquisition lasted 8 min and additional MRI sequences added approximately 12 min of table-time. This delayed module was executed independently.

3.2.3 Image Reconstruction and Fusion

PET reconstruction parameters including iterations, subsets, TOF, PSF, matrix, post-filter settings, and MR-based attenuation-correction (two-point Dixon) are documented in Table 1. The dedicated 8-channel breast array coil was incorporated within the MR-based μ-map for prone-position attenuation correction. Attenuation-corrected PET and MRI datasets were exported to the AW 4.6 workstation for off-line co-registration and fusion.

3.3 Image Analysis

Two radiologists (each ≥ 10 years of experience, associate-professor level or higher) interpreted all datasets. Readers were blinded to histopathological results. Disagreements between the two readers were resolved by a senior radiologist. Inter-reader agreement metrics (κ for categorical lesion classification, ICC for ADCmin and SUVmax) were calculated and the number of adjudicated cases is reported.

3.3.1 Diagnostic Criteria [7]

MRI morphological criteria for benign and malignant lesions were defined according to ACR BI-RADS-MRI 5th-edition lexicon.

Benign MRI features: T1 iso- to mildly-hypointense, T2 hyperintense, smooth margins, regular shape, absent lobulation or spiculation, no skin retraction, DWI iso- to mildly-hyperintense, ADC iso- to mildly-hypointense.

Malignant MRI features: mass demonstrating lobulation or spiculation, irregular/ill-defined margins, architectural distortion, adjacent skin thickening or

nipple retraction, T1 iso- to low-signal, T2 mildly-hyperintense, markedly elevated DWI signal, reduced ADC values.

PET visual positivity criterion: ^{18}F-FDG uptake greater than adjacent breast background parenchyma; we acknowledge this visual criterion is relatively lenient and may produce equivocal findings in inflammatory or proliferative breast tissue.

For the MSDP-MS assessment, readers integrated early-phase PET, delayed-phase PET, multi-sequence MRI (T1, T2, STIR, DWI-derived ADC), and fused PET/MRI datasets to assign binary benign/malignant classification. For conventional-PET/MRI assessment, readers evaluated only the early-phase supine torso-coil PET/MRI dataset.

3.3.2 Quantitative Parameters

ADCmin: On ADC maps, a manual semi-automatic ROI (AW 4.6 Breast ROI Assist tool) was placed guided by the voxel demonstrating simultaneously highest SUVmax and lowest ADC signal. ROIs were restricted to solid tumour parenchyma while avoiding cystic or necrotic components. Per-lesion ROI area and voxel counts were recorded. Both ADCmin and ADC-10th-percentile values were documented. In multifocal disease, the lesion demonstrating the highest FDG avidity was selected for quantitative measurement. ADCmin values obtained on delayed-phase datasets were recorded. SUVmax: Maximum standardized-uptake value was measured on both early-phase and delayed-phase PET datasets.

ΔSUVmax%: Percentage-change of SUVmax from early-phase to delayed-phase.

$$\Delta SUVmax\% = [(SUVmax_delayed - SUVmax_early) / SUVmax_early] \times 100\ \%.$$

3.4 Statistical Analysis

Statistical analyses were performed with SPSS 28.0. Categorical variables are summarised as counts (percentages). Group comparisons used χ^2 or Fisher's exact test. Continuous variables are expressed as median [inter-quartile range] or mean ± SD as appropriate and normality was assessed with Shapiro-Wilk testing. Groups were compared with independent-samples t-test (normally-distributed data) or Mann-Whitney U-test (non-normal / small subgroups). Diagnostic performance indices (sensitivity, specificity, accuracy, PPV, NPV) for the two binary-classification reading outputs were calculated from 2 × 2 contingency tables. Paired comparison of performance indices used McNemar's test, with discordant-pair counts explicitly reported. Because only binary benign-versus-malignant outputs were obtained, formal ROC-curve construction was not feasible. Optimal cut-off values for quantitative parameters were derived using the Youden-index within the present dataset. Bootstrap resampling (1000 replicates) was used to compute 95 % confidence intervals for cut-off estimates. The Wilson-score method was used to calculate 95 % confidence intervals for diagnostic indices. Statistical significance threshold was set at $\alpha = 0.05$.

4 Results

4.1 Lesion Characteristics

Among 68 enrolled patients, 63 demonstrated solitary lesions and 5 patients had multifocal breast disease; for multifocal cases, the most FDG-avid lesion was selected for quantitative analysis. According to histopathology, 44 lesions were benign and 24 lesions were malignant.

Lesion-size distribution: 0-1 cm (n = 14), 1-2 cm (n = 28), 2-3 cm (n = 12), 3-4 cm (n = 6), > 4 cm (n = 8). Early-phase SUVmax for benign lesions ranged 0.2-3.1; malignant-lesion early-phase SUVmax ranged 2.5-18.7.

4.2 Diagnostic Performances

Conventional early-only PET/MRI correctly classified 56 out of 68 lesions (18 true-positive, 38 true-negative) and 12 lesions were misclassified (6 false-negative, 6 false-positive) (Table 2).

MSDP-MS correctly classified 64 of 68 lesions (22 true-positive, 42 true-negative) and 4 lesions were misclassified (2 false-negative, 2 false-positive) (Table 3 and Figure 1).

FIGURE 1 The comparison of the diagnostic accuracy rates between conventional PET/MRI and MSDP-MS.

Diagnostic metrics with 95 % Wilson-score confidence intervals and McNemar-test statistics (including discordant-pair counts b and c) are summarised in Table 4.

4.3 Delayed-Phase Characteristics

4.3.1 ^{18}F-FDG Uptake Change

Delayed-phase SUVmax increased in 37/68 lesions (54.41 %): 18 malignant lesions, 19 benign lesions.

Delayed-phase SUVmax decreased in 31/68 lesions (45.59 %): 6 malignant lesions, 25 benign lesions.

4.3.2 ADCmin Values

SUVmax-decrease subgroup (n = 31):

Benign ADCmin: $1.52 \pm 0.18 \times 10^{-3}$ mm²/s.

Malignant ADCmin: $1.15 \pm 0.21 \times 10^{-3}$ mm²/s.

Exploratory Youden-index-derived cut-off = 1.31×10^{-3} mm²/s.

SUVmax-increase subgroup (n = 37):

Benign ADCmin: $1.08 \pm 0.21 \times 10^{-3}$ mm²/s.

Malignant ADCmin: $0.82 \pm 0.15 \times 10^{-3}$ mm²/s.

Exploratory Youden-index-derived cut-off = 0.86×10^{-3} mm²/s.

Figure 2 illustrated that the SUVmax-decrease group showed a broad ADCmin spread without a sharp peak, skewing toward higher value consistent with the benign histology (Figure 3). In contrast, the SUVmax-increase group clusters at low ADCmin values, supporting the classic paradigm of "high metabolism + high cellularity = malignancy" (Figure 4). A secondary, smaller peak around 1.5×10^{-3} mm²/s likely reflected hypermetabolic and hypocellular lesions such as inflammation or malignant tumors with necrosis and cystic changes. This corresponded to the upper-right contradiction quadrant in Figure 5. When measuring the ADCmin the ROI should be placed at the site of the highest FDG metabolism within the lesion, avoiding cystic changes and necrotic areas. As shown in Figure 6, the ADCmin value of the FDG hypermetabolic area at the anterior edge of the lesion is 0.64×10^{-3} mm²/s, whereas that the FDG hypometabolic area at the posterior edge was 1.47×10^{-3} mm²/s. Incorrect selection of the measurement position can easily lead to misjudgment.

FIGURE 2 The distribution pattern of the ADCmin value.

FIGURE 3 A 40-year-old woman with a right axillary ectopic breast tissue showed the florid ductal papillomatous hyperplasia.

A:Early-phase T2 shows an ill-defined hyperintense focus in the upper-outer quadrant with increased FDG uptake (SUVmax = 2.60). B:DWI reveals mildly elevated signal. C:Delayed-phase FDG uptake decreases (SUVmax = 2.36). D:ADC map shows mildly reduced signal. ADCmin = 1.31 × 10^{-3} mm^2/s. E:Histopathology of the lesion.

FIGURE 4 A 47-year-old woman with a grade II invasive ductal carcinoma in the upper-outer quadrant of the right breast.

A:Early-phase imaging: T1 isointense, T2 hyperintense mass; mild FDG uptake (SUVmax = 1.23). B:Delayed-phase imaging: FDG uptake slightly increases (SUVmax = 1.39); DWI shows high signal. C:Early-phase DWI also demonstrates high signal. D:ADC map reveals reduced signal. ADCmin = 0.79 × 10^{-3} mm^2/s. E:Histopathology of the lesion.

FIGURE 5 Two-dimensional decision-space plot.

Note:Two decision boundaries: a. FDG threshold: (1) 0. (2) area above indicates increased metabolism, area below indicates decreased metabolism. b. ADC threshold: (1) 1.09 × 10^{-3} mm^2/s (median-based). (2) left of the line denotes malignant-suspicious zone, right denotes benign-predisposed zone. Four decision quadrants: a. Upper-left: high-risk malignant zone. b. Lower-right: high-confidence benign

zone.c. Lower-left: discordant zone—low-grade malignancies may show decreased metabolism, whereas densely packed benign proliferations may fall here. d. Upper-right: discordant zone—e.g., inflammatory lesions with loose cellularity (high ADC) yet intense FDG uptake can mimic malignancy; similarly, low-grade or necrotic/cystic tumors may reside here.

FIGURE 6 A 60-year-old woman with a grade II invasive carcinoma in the upper-outer quadrant of the right breast.

A:Delayed-phase PET/MRI shows markedly increased and heterogeneous FDG uptake (SUVmax = 15.93); DWI demonstrates high signal intensity. B:T1 isointense, T2 hyperintense mass. The anterior margin displayed intense FDG uptake.C: ADCmin measured in the FDG-avid region: 0.64×10^{-3} mm^2/s. D:ADCmin measured in the FDG-poor region: 1.47×10^{-3} mm^2/s. E:T1 isointense and T2 heterogeneous hyperintense signal throughout the lesion. F:Early-phase imaging shows elevated FDG uptake (SUVmax = 10.46). G:Histopathology of the lesion.

Based on the above results, the following conclusions could be drawn:

1. The median ADCmin is markedly lower in the SUVmax-increase group.

2. The bimodal distribution in the SUVmax-increase group underscored the need for the multiparametric diagnosis, as some hypermetabolic false-positive lesions (e.g., inflammation) retained the relatively high ADCmin values.

3. The overlap between the two groups confirmed that any single indicator had limitations, so the multidimensional models such as the decision-space plot were required.

In conclusion, in the delayed-phase imaging, ΔSUVmax% offers the modest utility for the malignancy assessment within the FDG-uptake-increase group, especially when the increment exceeds 56.4%. Its value was limited in the FDG-uptake-decrease group. In the FDG-uptake-increase group the ADCmin cut-off 0.86×10^{-3} mm²/s yielded AUC 0.88 (95 % CI 0.79–0.95) and a Youden index of 0.73 (sensitivity 89.2 %, specificity 83.8 %). In the FDG-uptake-decrease group, the ADCmin cut-off 1.31×10^{-3} mm²/s yielded AUC 0.92 (95 % CI 0.85–0.98) and a Youden index of 0.81 (sensitivity 87.5 %, specificity 93.5 %). Regardless of FDG trend, the malignant nodules had significantly lower ADCmin values ($P<0.05$). Among them, the ADCmin values of the malignant nodules in the FDG-uptake-increase group were on average 24.1% lower than that of benign nodules, and in the FDG-uptake-decrease group they were 24.3% lower. When ADCmin < 1.31×10^{-3} mm²/s, the probability of malignancy exceeded 90%. By combining the ADCmin value with the morphological features of nodules such as unclear boundaries, spicules, and lobulation, a nodule can be basically determined to be malignant. In the FDG-uptake-decreased group (n = 31), MSDP-MS increased the diagnostic specificity to 92.0% (23/25), while in the FDG-uptake-increased group (n = 37), MSDP-MS increased the diagnostic specificity to 90.5% (19/21), underscoring the need for the metabolic-subgroup analyses in the future studies.

4.3.3 ΔSUVmax% Analysis

In the FDG-uptake-increase group, the mean change rate of ΔSUVmax in the pathological benign lesions was 29.94 ± 32.91%, and in the pathological malignant

lesions it was 47.67 ± 60.64%.

5 Discussion

Breast cancer represents a major malignancy affecting women. Ultrasound, mammography, CT and MRI are widely applied given favourable accessibility and cost-performance, yet each modality carries well-recognised limitations [8-10]. PET/MRI provides high-quality multiparametric information but is associated with higher cost and technical complexity; its value in breast-lesion characterisation continues to be investigated.

The present work explores a combined early-plus-delayed prone breast-coil PET/MRI workflow for BI-RADS 4 nodule assessment. Conventional supine torso-coil PET/MRI can be limited by high background parenchymal metabolic activity, suboptimal breast spatial resolution, and DWI-ADC measurement distortion related to breast compression. The MSDP-MS combined dataset integrates three major components: (1) Dual-time-point FDG metabolic imaging exploiting potential differential wash-out behaviour between breast parenchyma and tumour tissue[11-12]. (2) Prone-position dedicated-breast-coil acquisition to improve anatomical visualisation and reduce compression-related artefacts. (3) Multi-sequence MRI complementing PET metabolic information[13-15].

Compared with early-phase-only supine PET/MRI, the combined MSDP-MS dataset increased the diagnostic accuracy (82.4% vs. 94.1%, P =0.025) and the

diagnostic sensitivity (75.0 % vs. 91.7 %, P =0.041). Specificity and NPV increased by 9.1% respectively, but after Bonferroni correction the difference between them were not statistically significant (P = 0.108).

This study showed that the false positive rate of conventional PET/MRI was 13.6%, while that of MSDP-MS was 4.5%, indicating a reduction in the false positive rate of MSDP-MS. Combining ADCmin thresholds (< 0.86 × 10^{-3} mm^2/s gives > 90 % malignancy probability) with the morphologic features provided the dual safeguards against the unnecessary biopsy and under-diagnosis. MSDP-MS could prevent unnecessary biopsies of 9.1% of benign nodules and enable early intervention for 16.7% of malignant nodules, which has important clinical practical value. Exploratory analysis revealed that 4/24 (16.7 %) malignant cases had potential up-staging, aligning with the research results of Jannusch et al.[9] who reported that PET/MRI had altered the managements in 32.7 % of breast cancer patients, with 28.1 % of those changes due to stage changes. High-resolution PET/MRI in the delay period can detect the tiny metastases that are missed by conventional scans, such as lymph nodes < 0.5 cm in diameter. The combined analysis of ADCmin value and ΔSUVmax% could reduce the false positive stage of benign hyperplastic lymph nodes.

Several prior publications have described prone dedicated-breast-coil PET/MRI protocols, including Kirchner et al. [16], who compared one-step whole-body PET/MRI versus two-step protocols incorporating prone breast-coil imaging. Kirchner reported that the diagnostic specificity rose from 82 % to 89 %, matching

our results (from 86.4 % to 95.5 %). Both studies demonstrated the value of delayed imaging in reducing biopsies of benign nodules. This study aligns with the research direction of Van Nijnatten on optimizing the PET/MRI breast scanning process [17]. However, this study innovatively combined a 3-hour delayed-time-point with subgroup-specific ADCmin exploratory thresholds.

In terms of technical details, this study reached the following conclusions: (1)for small nodules, T2-Propeller outperformed T1-LAVA. (2) DWI sequences, especially those with high b values and high excitation numbers, were more sensitive to nodule detection. (3) Measuring the ADCmin value was more significant than measuring the average ADC value (ADCavg) for differentiating benign and malignant nodules. It should be emphasized that an increase in SUVmax on the delayed imaging is not an independent diagnostic criterion for the malignant lesions. A comprehensive judgment must be made in combination with the morphological and functional features of MRI (such as ADC values).

6 Conclusions

The combined MSDP-MS multiparametric PET/MRI dataset integrating early-phase supine acquisition and a 3-hour delayed prone dedicated-breast-coil acquisition demonstrated promising exploratory diagnostic performance for differentiating benign and malignant BI-RADS 4 breast nodules in this study. Future research directions include: (1) larger cohort enrolment (target $n \geq 200$ including ≥ 120 benign lesions) to validate subgroup diagnostic indices. (2) Sequence-optimisation and stratified-analysis according to lesion metabolic patterns.

(3) Further evaluation of this workflow for calcified /cyst-containing breast lesions and for breast-cancer therapy-response assessment via multi-centre cohorts. (4) Integration of artificial-intelligence approaches to refine combined ADC-SUV-based diagnostic models.

7 References

1. Gradishar WJ, Moran MS, Abraham J, Aft R, Agnese D, Allison KH, et al. NCCN Clinical Practice Guidelines in Oncology: Breast Cancer, Version 3.2.22. J Natl Compr Canc Netw. 2022;20(5):691-722. doi: 10.6004/jnccn.2022.0030.

2. Coffey K, Jochelson MS. Contrast-enhanced mammography in breast cancer screening. Eur J Radiol. 2022;156:110513. doi: 10.1016/j.ejrad.2022.110513.

3. Wekking D, Porcu M, De Silva P, Saba L, Scartozzi M, Solinas C. Breast MRI: clinical indications, recommendations, and future applications in breast cancer diagnosis. Curr Oncol Rep. 2023;25(4):257-67. doi: 10.1007/s11912-023-01372-x.

4. Nicholson WK, Silverstein M, Wong JB, Barry MJ, Chelmow D, Coker TR, et al. Screening for breast cancer: US Preventive Services Task Force recommendation statement. JAMA. 2024;331(22):1918-30. doi: 10.1001/jama.2024.5534.

5. Bruckmann NM, Morawitz J, Fendler WP, Ruckhäberle E, Bittner AK, Giesel FL, et al. A role of PET/MRI in breast cancer. Semin Nucl Med. 2022;52(5):611-8.doi: 10.1053/j.semnuclmed.2022.01.003.

6. Fowler AM, Strigel RM. Clinical advances in PET-MRI for breast cancer. Lancet Oncol. 2022;23(3):e32-e43. doi: 10.1016/S1470-2045(21)00577-5.

7. American College of Radiology. BI-RADS-Atlas, 5th edition: MRI lexicon. Reston, VA: ACR; 2020.

8. Choi JH, Kim HA, Kim W, Lim I, Lee I, Byun BH, et al. Early prediction of neoadjuvant chemotherapy response for advanced breast cancer using PET/MRI image deep learning. Sci Rep. 2020;10(1):21149. doi: 10.1038/s41598-020-77875-5.

9. Jannusch K, Umutlu L, Kirchner J, Bruckmann NM, Morawitz J, Herrmann K, et al. Impact of ^{18}F-FDG PET/MRI on therapeutic management of women with newly diagnosed breast cancer: results from a prospective double-center trial. J Nucl Med. 2024;65(12):1855-61. doi: 10.2967/jnumed.124.268065.

10. Morawitz J, Bruckmann NM, Dietzel F, Ullrich T, Bittner A, Hoffmann O, et al. Determining the axillary nodal status with 4 current imaging modalities, including ^{18}F-FDG PET/MRI, in newly diagnosed breast cancer: a comparative study using histopathology as the reference standard. J Nucl Med. 2021;62(10):1677-83. doi: 10.2967/jnumed.121.262009.

11. Kim HO, Kim BS, Kang SY, Bang KI, An J, Kim JH, et al. Metabolic changes in breast cancer on dual-time-point ^{18}F-FDG PET/CT imaging according to primary tumour uptake and background parenchymal enhancement. Ann Nucl Med. 2020;34(12):942-51. doi:10.1007/s12149-020-01525-z.

12. Fang N, Wang XY, Zeng L. Dual-phase dual-position ^{18}F-FDG PET/CT imaging improves visualisation of T1 breast-cancer lesions. J Clin Radiol. 2019;38(8):1391-4.

13. Bruckmann NM, Kirchner J, Morawitz J, Umutlu L, Herrmann K, Bittner AK, et al. Prospective comparison of CT and ^{18}F-FDG PET/MRI in N and M staging of

primary breast-cancer patients: initial results. PLoS One. 2021;16(12):e0260804. doi: 10.1371/journal.pone.0260804.

14. Romeo V, Clauser P, Rasul S, Kapetas P, Gibbs P, Baltzer PAT, et al. AI-enhanced simultaneous multiparametric ^{18}F-FDG PET/MRI for accurate breast-cancer diagnosis. Eur J Nucl Med Mol Imaging. 2022;49(2):596-608. doi: 10.1007/s00259-021-05492-z.

15. Umutlu L, Kirchner J, Bruckmann NM, Morawitz J, Antoch G, Ingenwerth M, et al. Multiparametric integrated ^{18}F-FDG PET/MRI-based radiomics for breast-cancer phenotyping and tumour decoding. Cancers (Basel). 2021;13(12):2928. doi: 10.3390/cancers13122928.

16. Kirchner J, Grueneisen J, Martin O, Oehmigen M, Quick H, Bittner AK, et al. Local and whole-body staging in patients with primary breast-cancer: a comparison of one-step to two-step staging utilizing ^{18}F-FDG-PET/MRI. Eur J Nucl Med Mol Imaging. 2018;45(13):2328-37. DOI:10.1007/s00259-018-4102-4.

17. Van Nijnatten TJA, de Mooij CM, Mitea C, Houwers J, de Boer M, Smidt ML, et al. ^{18}F-FDG whole-body PET-MRI including an integrated breast-MRI protocol for locoregional and distant staging in breast-cancer patients-a feasibility study. Insights Imaging. 2024;15(1):123. DOI:10.1186/s13244-024-01830-5.

Acknowledgments:

The authors declare that no funds, grants, or other support were received during the preparation of this manuscript. The authors have no relevant financial or non-financial interests to disclose.

	Scanning Sequence	Slice Thickness (mm)	Slice Gap (mm)	TE (ms)	TR (ms)	FOV (cm)	NEX	b Value (s/mm²)
Early Imaging （p.i.50 min later）	Ax Fs T2 Propeller	6.0	1.5	71	11250	44.0	2.0	-
Chest Coil （3.0T UAA 16 channel）	Ax T1 LAVA Flex	4.8	1.5	min full	4.4	44.0	1.0	-
	Ax DWI 800 shim	4.0	1.5	69.6	7500	40	2.0	800
Delayed imaging （p.i.3 hours later）	Ax STIR DWI 1000 shim	4.0	1.0	minimum	3567.9	40	4.0	800, 1000
Breast-specific coil （3.0T HD flat gem table breast array 8 channel）	Ax T2 FSE Ideal Asset	4.0	1.0	85	4688	40	1.0	-
	Ax T1 FSE	4.0	1.0	min full	420	40	1.0	-
	Sag Fs T2 FSE	4.0	1.0	85	3000	40	2.0	-

Note: DWI acquisitions included $b = 800$ for early-phase scans and $b = 800, 1000$ for delayed-phase scans; no separate $b = 0$ acquisition was performed. ADC computation limitations are acknowledged in the Limitations subsection. SUV values were normalised to body weight.

Table 2 The lesions pathologies vs. the diagnostic performances of conventional PET/MRI.

	Malignant (Imaging)	Benign (Imaging)
Malignant	18	6
Benign	6	38
Total	24	44

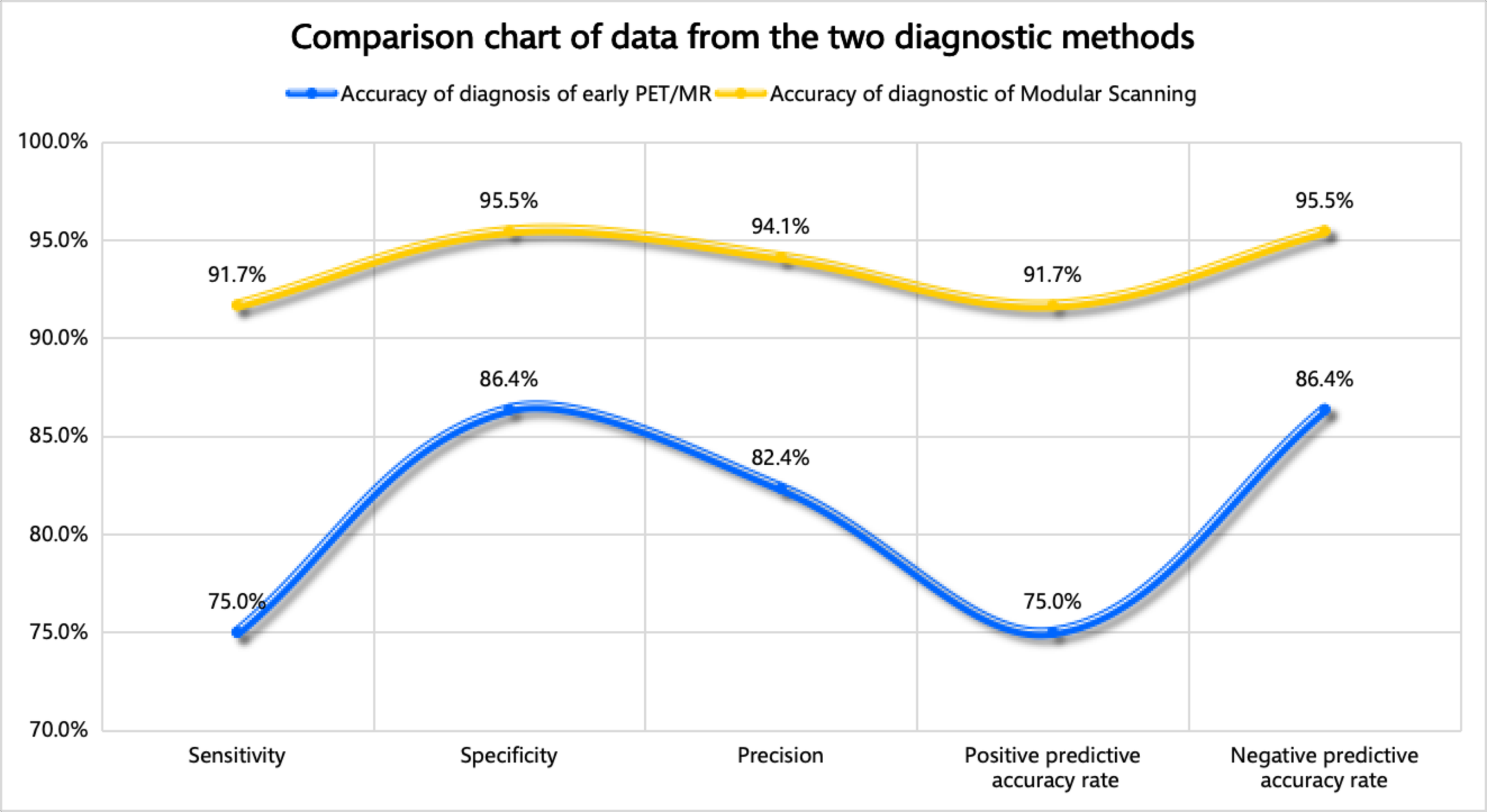
Table 3 The lesions pathologies vs. the diagnostic performances of MSDP-MS.

	Malignant (MSDP-MS)	Benign (MSDP-MS)
Malignant	22	2
Benign	2	42
Total	24	44

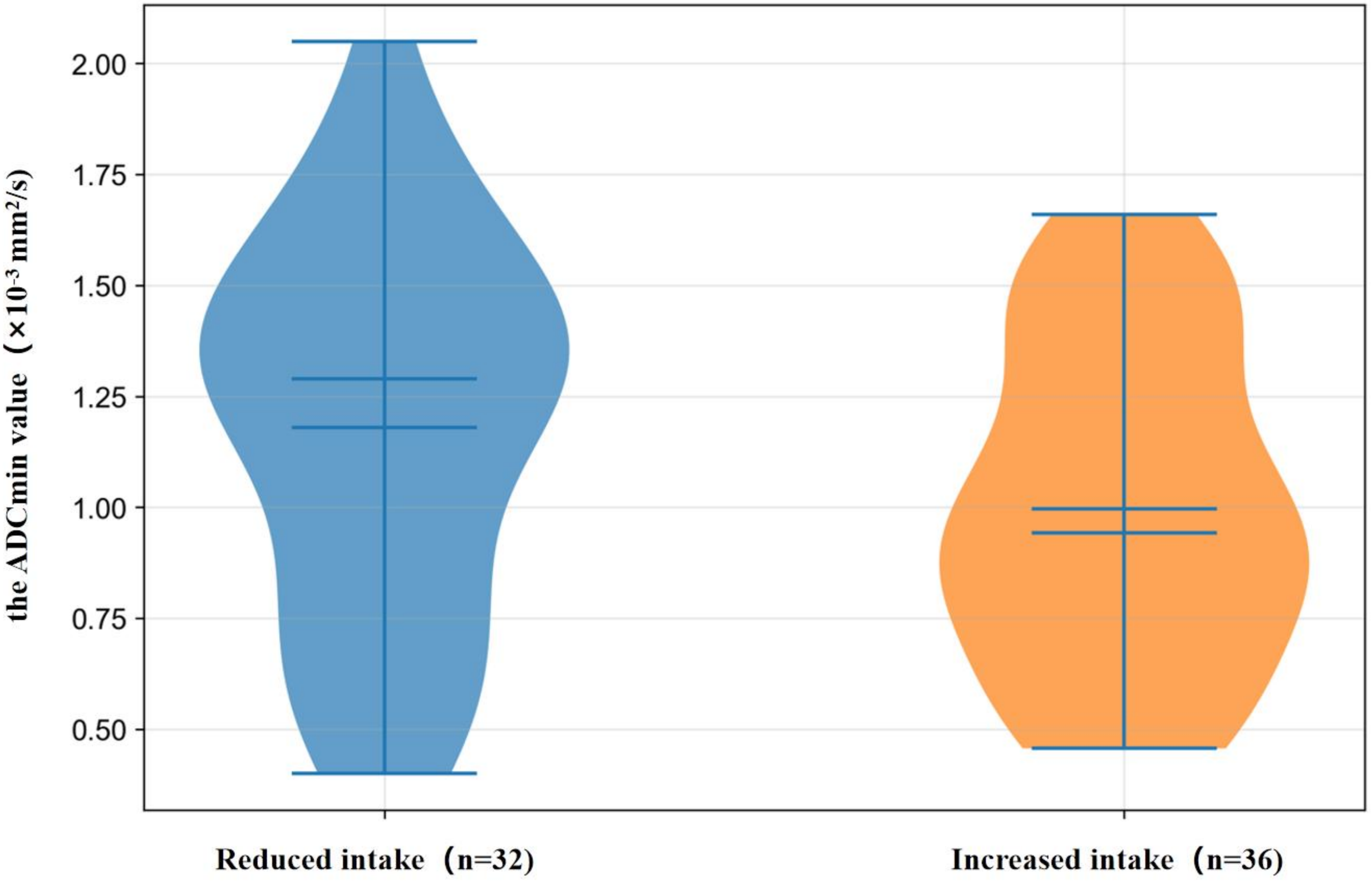
Table 4 The comparison of the diagnostic performances between conventional PET/MRI and MSDP-MS.

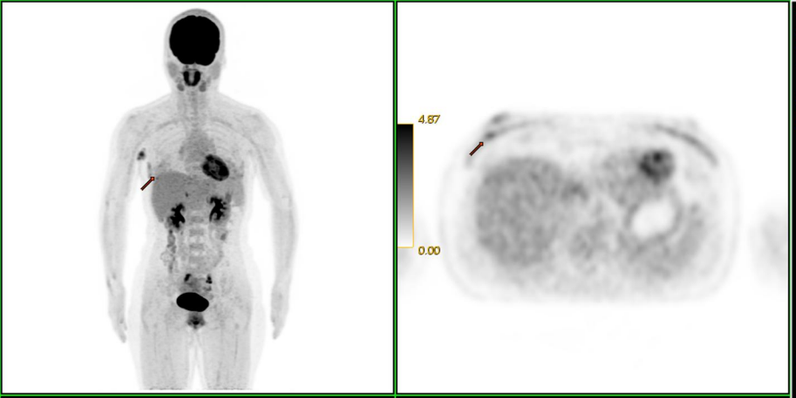
	Conventional PET/MRI	MSDP-MS	X^2	P
Sensitivity（%，95%CI）	75.0（58.5-87.9）	91.7（82.3-98.5）	4.17	0.041
Specificity（%，95%CI）	86.4（73.7-94.3）	95.5（86.2-99.5）	2.58	0.108
Accuracy（%，95%CI）	82.4（71.5-90.6）	94.1（85.8-98.9）	5.02	0.025
PPV（%，95%CI）	75.0（58.5-87.9）	91.7（82.3-98.5）	4.17	0.041
NPV（%，95%CI）	86.4（73.7-94.3）	95.5（86.2-99.5）	2.58	0.108

Abbreviations: PPV = positive predictive value. NPV = negative predictive value.

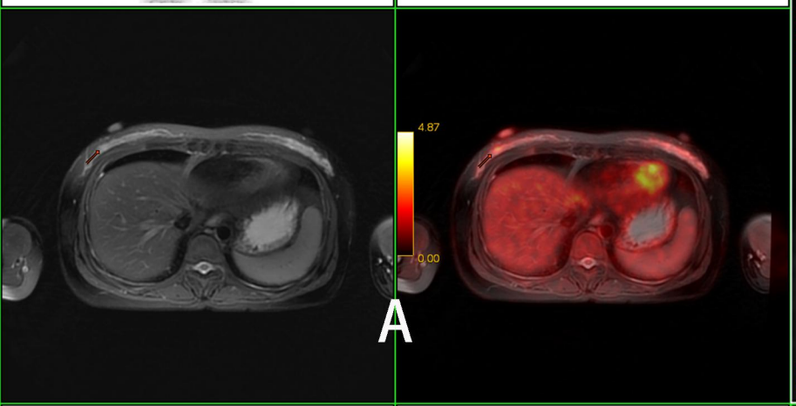

Comparison chart of data from the two diagnostic methods
Accuracy of diagnosis of early PET/MR
Accuracy of diagnostic of Modular Scanning
100.0%
95.0%
90.0%
85.0%
80.0%
75.0%
70.0%
91.7%
95.5%
94.1%
91.7%
95.5%
75.0%
86.4%
82.4%
75.0%
86.4%
Sensitivity
Specificity
Precision
Positive predictive accuracy rate
Negative predictive accuracy rate

the Distribution Pattern of ADCmin Value



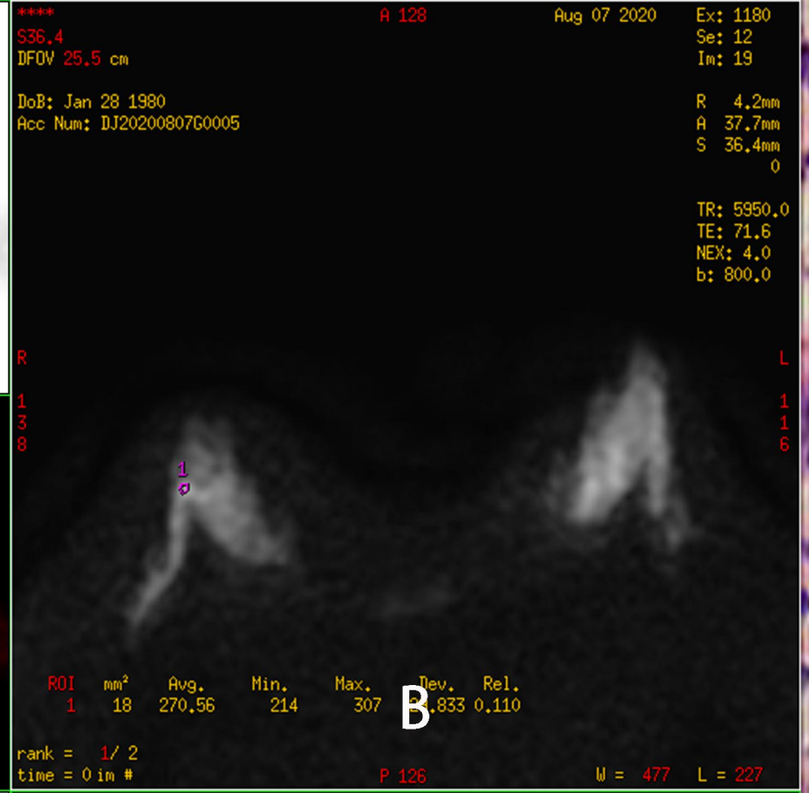


4.87
0.00

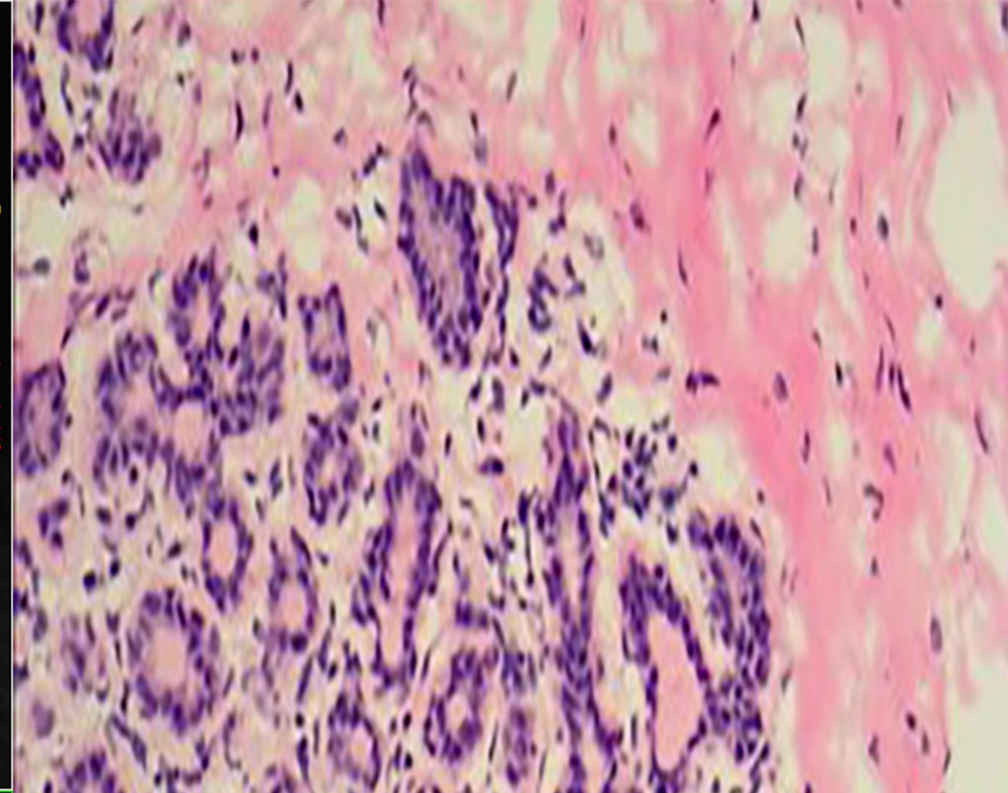


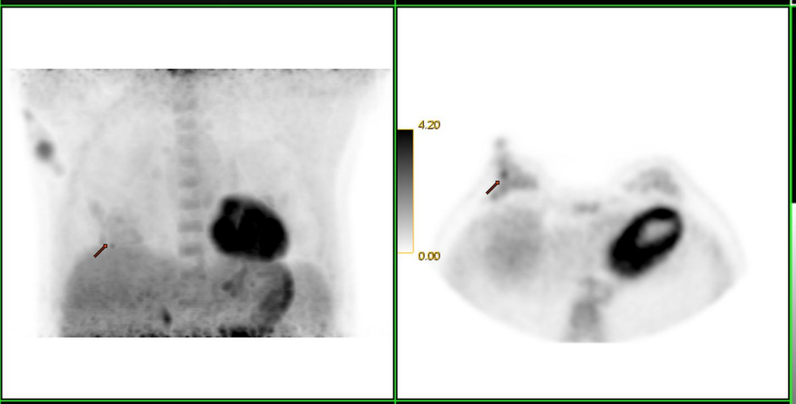
4.87
0.00

A

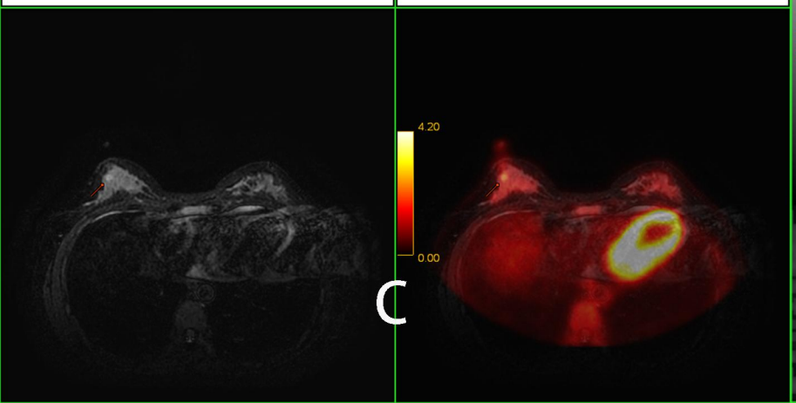

**** A 128 Aug 07 2020 Ex: 1180
S36.4 Se: 12
DFOV 25.5 cm Im: 19
DoB: Jan 28 1980 R 4.2mm
Acc Num: DJ2020080760005 A 37.7mm
S 36.4mm
0
TR: 5950.0
TE: 71.6
NEX: 4.0
b: 800.0
R L
1 1
3 1
8 6
1
ROI mm² Avg. Min. Max. Dev. Rel.
1 18 270.56 214 307 .833 0.110
rank = 1/ 2
time = 0 im #
P 126 W = 477 L = 227

B



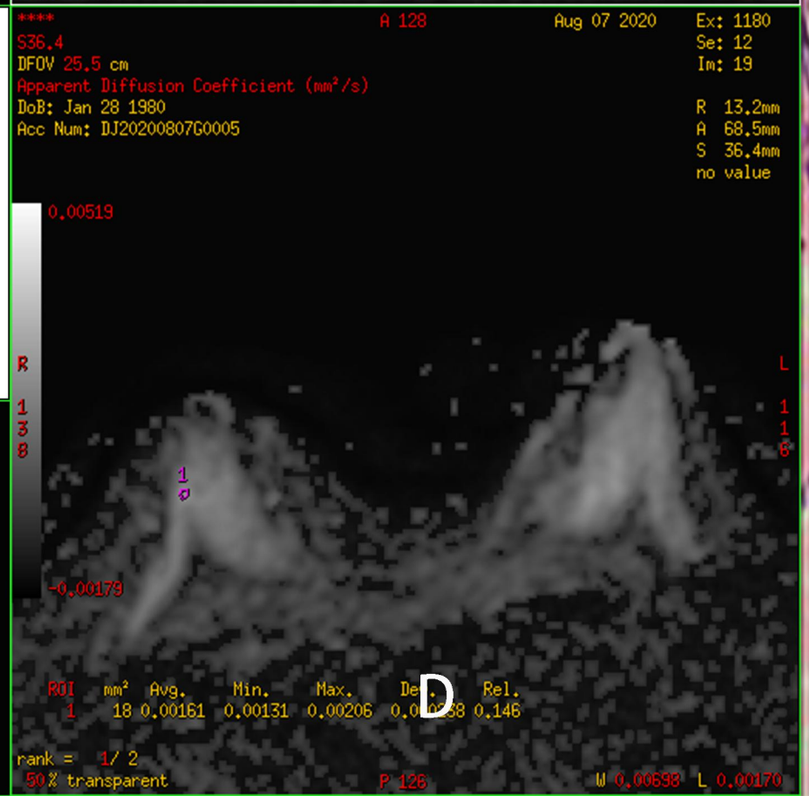


4.20
0.00

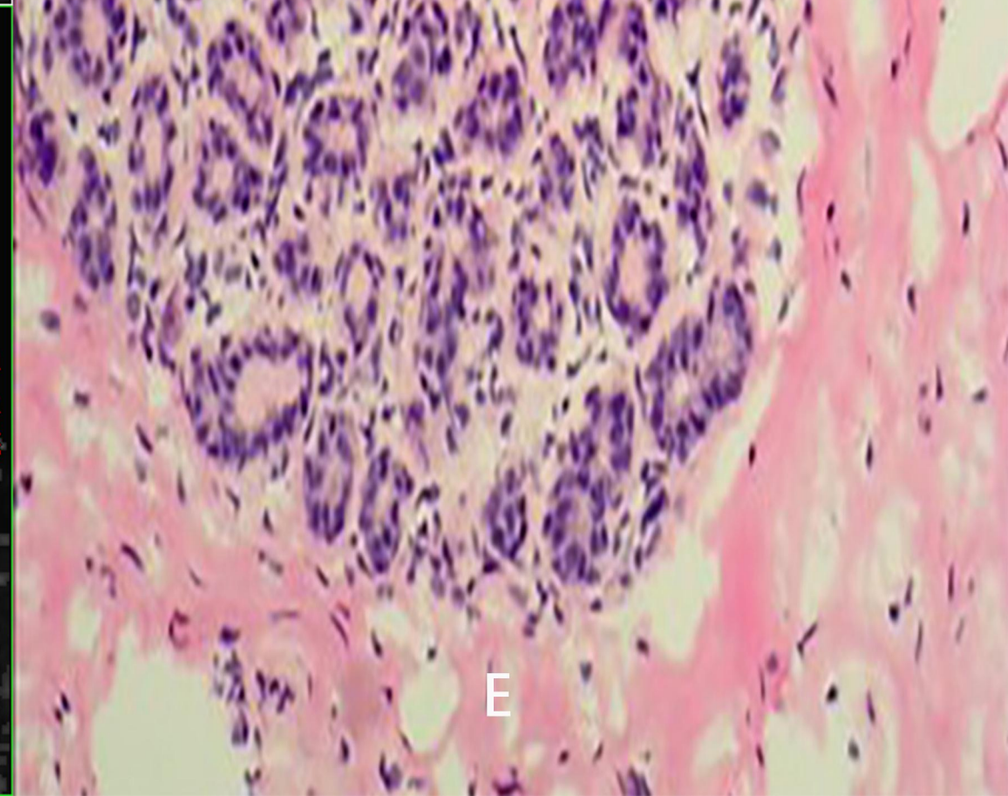


4.20
0.00

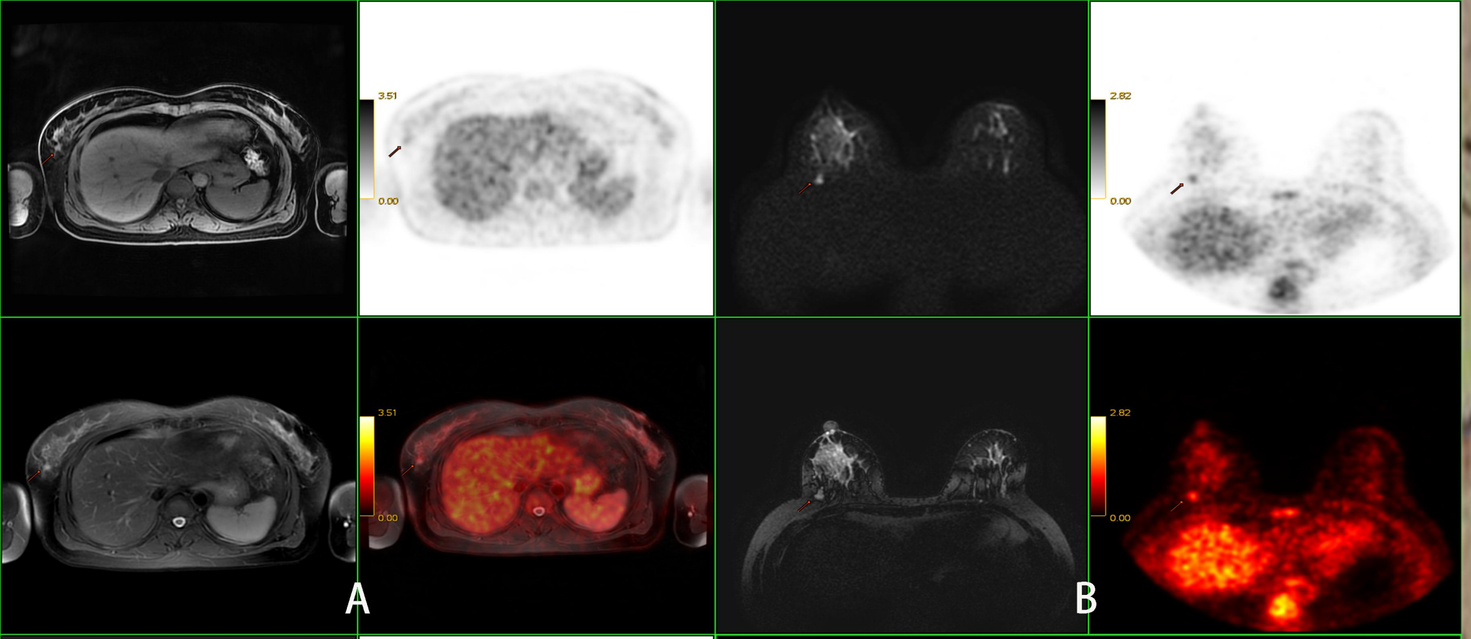
C

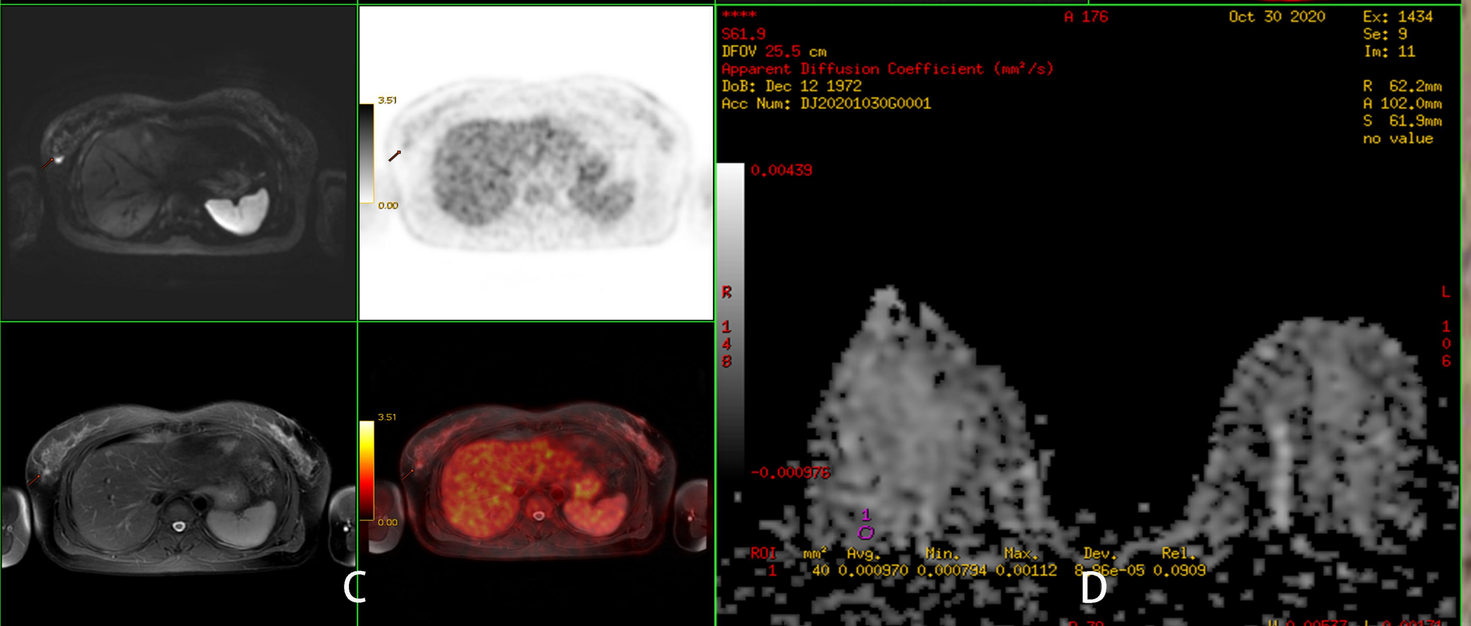

**** A 128 Aug 07 2020 Ex: 1180
S36.4 Se: 12
DFOV 25.5 cm Im: 19
Apparent Diffusion Coefficient (mm²/s)
DoB: Jan 28 1980 R 13.2mm
Acc Num: DJ2020080760005 A 68.5mm
S 36.4mm
no value
0.00519
R L
1 1
3 1
8 6
1
-0.00179
ROI mm² Avg. Min. Max. De . Rel.
1 18 0.00161 0.00131 0.00206 0.0 38 0.146
rank = 1/ 2
50% transparent
P 126 W 0.00698 L 0.00170

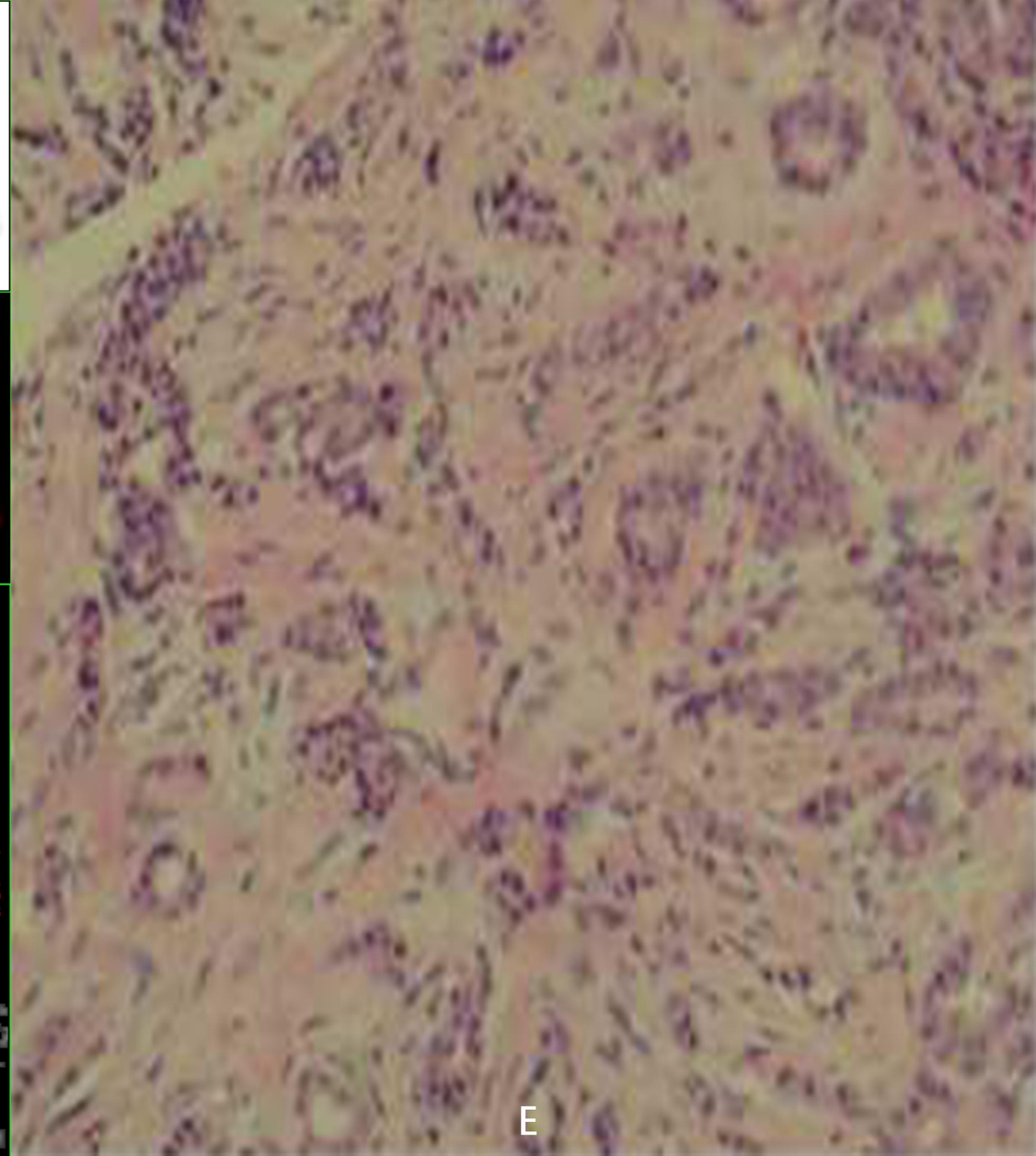
D

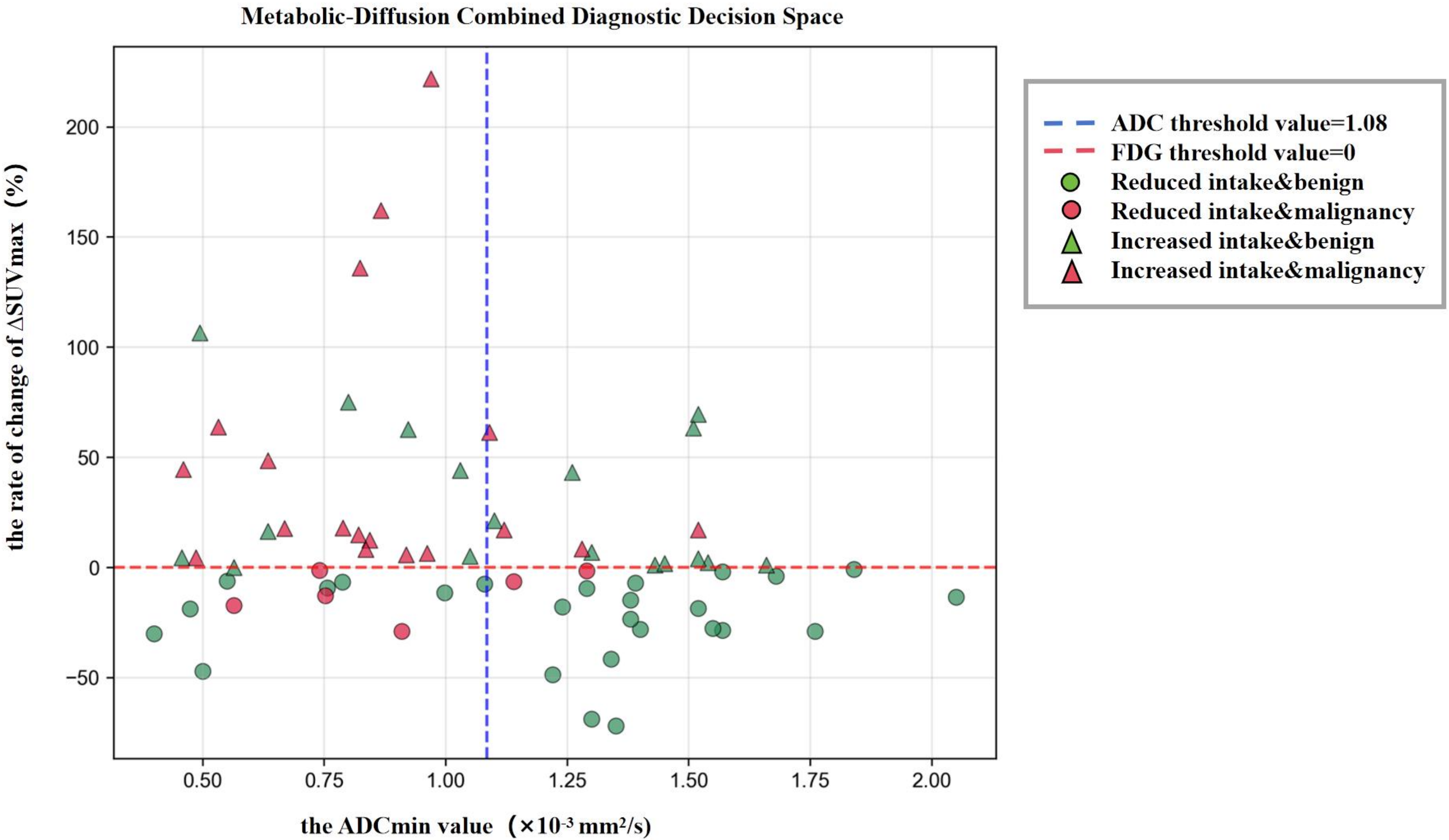


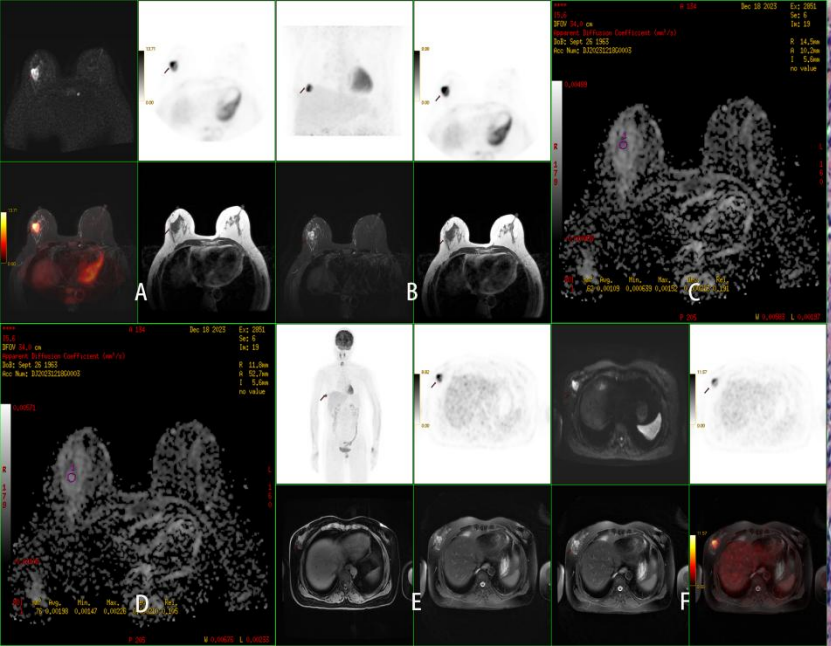
E


3.51
0.00
2.82
0.00
A
B


3.51
0.00
C
****
S61.9
DFOV 25.5 cm
Apparent Diffusion Coefficient (mm²/s)
DoB: Dec 12 1972
Acc Num: DJ20201030G0001
A 176
Oct 30 2020
Ex: 1434
Se: 9
Im: 11
R 62.2mm
A 102.0mm
S 61.9mm
no value
0.00439
-0.000976
R
148
L
106
1
ROI mm² Avg. Min. Max. Dev. Rel.
1 40 0.000970 0.000794 0.00112 8.36e-05 0.0909
D


E


Metabolic-Diffusion Combined Diagnostic Decision Space
the rate of change of ΔSUVmax (%)
200
150
100
50
0
−50
0.50
0.75
1.00
1.25
1.50
1.75
2.00
the ADCmin value (×10-3 mm2/s)
ADC threshold value=1.08
FDG threshold value=0
Reduced intake&benign
Reduced intake&malignancy
Increased intake&benign
Increased intake&malignancy


A
B
C
D
E
F
G